Journal of Cardiovascular Magnetic Resonance (2005) **7,** 693–703
Copyright © 2005 Taylor & Francis Inc.
ISSN: 1097-6647 print / 1532-429X online
DOI: 10.1081/JCMR-200065637

Taylor & Francis
Taylor & Francis Group

VENTRICULAR FUNCTION

Accelerated tagging for the assessment of left ventricular myocardial contraction under physical stress

SALOME RYF,[1] JUERG SCHWITTER,[2] MARCUS A. SPIEGEL,[1] ANDREA K. RUTZ,[1] ROGER LUECHINGER,[1] GÉRARD R. CRELIER,[1] and PETER BOESIGER[1,*]

[1]*Institute for Biomedical Engineering, University and ETH Zürich, Switzerland*
[2]*Division of Cardiology, University Hospital Zürich, Switzerland*

A TFEPI-CSPAMM sequence is introduced, which is optimized with respect to acquisition speed and image quality. The sequence is used in a stress study, where a short breath-hold duration is crucial, and tested for reproducibility of deformation parameters extracted by HARP for repeated measurements.

Key Words: Myocardial tagging; CSPAMM; TFEPI; HARP; Physiological stress; Reproducibility

1. Introduction

The investigation of cardiac function under pharmacological or physical stress is a widely accepted method in clinical cardiology for the diagnosis of ischemia (1–4). For physical exercise, clinically frequently used devices are the treadmill and the ergometer (5). The advantage of examinations under physically induced stress include the better resemblance of cardiovascular stress encountered in daily life. Further, it has been reported that physically induced stress performs equally well or even better than pharmacological stress with respect to sensitivity or specificity when investigating for coronary artery diseases (6).

During stress examination, cardiac function is typically monitored by echocardiography in order to detect ischemia-induced dysfunction. Alternatively, MRI has been used for function assessment during inotropic stress (7). Myocardial tagging, such as Spatial Modulation of Magnetization (SPAMM) (8) or Complementary SPAMM (CSPAMM) (9), is a powerful technique for assessing quantitative, time resolved tissue deformation parameters that may provide superior information content in regard to accuracy and significance when compared with usual assessment (10). Under pharmacologically induced stress, myocardial tagging has successfully been applied in several studies (11–13). Also MR measurements under physical stress have successfully been performed (7, 14).

Since physical exercise not only increases the heart rate but also enhances breathing, it is important to reduce the required breath-hold time for the stress tagging measurements to a minimum in order to reduce image artifacts. However, shortening of acquisition time at a given spatial resolution decreases the signal-to-noise ratio (SNR) and, hence, affects data quality and consequently the feasibility of an automatic data analysis. To address these problems, CSPAMM was combined with a Turbo-Field Echo-Planar Imaging (TFEPI) (15) technique. TFEPI is a very efficient readout technique, which combines the advantages of the EPI technique, i.e., a fast read-out, with a short echo time, which leads to a reduction of flow artifacts. With a TFEPI sequence, a line tagged SPAMM data-set can be acquired in one RR-interval. Even tough the acquisition time for CSPAMM is doubled compared to SPAMM, it was chosen to be applied in this study because it allows for compensating the long-axis contraction of the heart by a slice-following procedure (16) and additionally provides better tag-line persistence throughout the cardiac cycle.

The focus of the study was to develop a TFEPI-CSPAMM sequence, which on one hand requires only a short breath hold in order to enable measurements under stress condition and on the other hand, produces sufficiently high image quality allowing for a reproducible semi-automatic quantification of deformation parameters. In order to balance these antipodal requirements, the TFEPI-CSPAMM sequence was improved in two steps. First, the sequences were evaluated under rest condition with respect to image quality and reproducibility of deformation parameters extracted by a HARmonic Phase (HARP) (17) evaluation technique. For this

Received 15 April 2004; accepted 14 April 2005.
*Address correspondence to Peter Boesiger, Institute for Biomedical Engineering, University and ETH Zürich, Gloriastrasse 35, Zürich CH-8092, Switzerland; Fax: +41-1-632-11-93; E-mail: boesiger@biomed.ee.ethz.ch

Order reprints of this article at www.copyright.rightslink.com

purpose, a semi-automatic algorithm was developed, which reproducibly detects endo- and epicardial borders in the modulus part of the HARP image [HARM (18)], from which various parameters such as circumferential shortening of the centerline (cFS) can be derived. Second, the performance of the optimal TFEPI-CSPAMM sequence was tested during ergometer stress in a series of volunteer studies.

2. Methods

The MR measurements were performed on a commercial 1.5 T whole body scanner (Gyroscan Intera, Philips Medical Systems), equipped with a five-element cardiac phased-array coil for signal reception and a vectorcardiogram (VCG) (19) for R-wave detection. Written informed consent was obtained from all subjects according to the laws of the ethical committee of the hospital (Universitätsspital Zürich). The patient protocols were approved by the hospital ethical committee (Kantonsspital Chur, Universitätsspital Zürich).

2.1. *Tagging preparation*

For the CSPAMM tagging preparation, two 90° radio frequency (RF) pulses were used, interspersed by a tagging gradient for spatial magnetization modulation. The second RF pulse was either a +90° or a −90° pulse, thus producing either a positive or a negative sinusoidal modulation of the z-magnetization, respectively. The CSPAMM tagging scheme involved subtraction of the two images with the positive and the negative modulations, consequently yielding an image with a net modulation of twice the amplitude (9). Two CSPAMM images with orthogonal one-dimensional stripe patterns with 8 mm tag distance were acquired with a slice following technique (16). All sequences were performed without fat saturation preparation.

2.2. *TFEPI sequence optimization*

2.2.1. *Flip angle optimization*

In order to achieve a constant tagging contrast throughout the whole cardiac cycle, a flip angle optimization similar to the one introduced for EPI CSPAMM (20) was applied. For an EPI-CSPAMM sequence with n cine frames per cardiac cycle, the signal intensity I_k of the k^{th} ($k = 1...n$) frame is (9):

$$I_k \propto M_{ss} \cdot TAG(x,y) \cdot \exp(-\Delta t/T_1) \cdot \prod_{j=1}^{k-1} \cos(\alpha_j) \cdot \sin(\alpha_k) \quad (1)$$

where

M_{ss} stands for steady state magnetization,

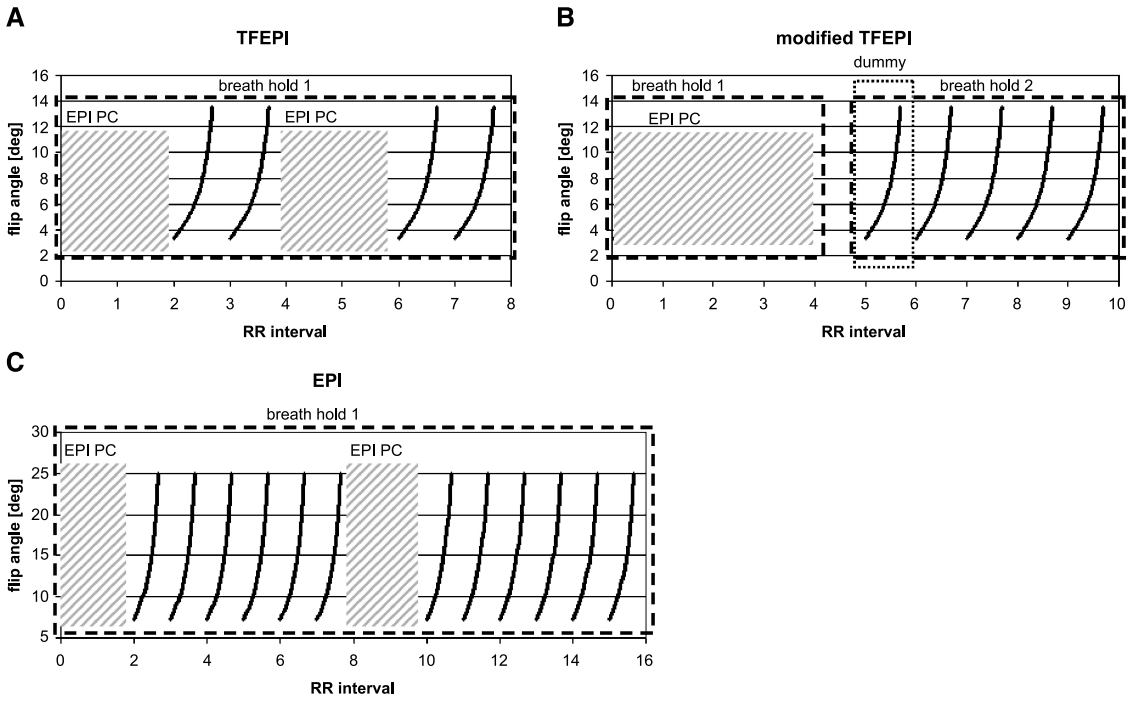

Figure 1. A: TFEPI sequence, B: modified TFEPI sequence, C: EPI sequence. In order to achieve a constant tagging contrast, the excitation flip angles are ramped. In the modified TFEPI sequence EPI-phase correction (EPI PC) is performed in a separate breath hold before the image acquisition and a dummy image acquisition is performed in order to achieve a better steady state. This leads to two breath holds of 4 and 5 RR-intervals respectively (B). In the TFEPI- (A) and the EPI-sequence (C), imaging is intercepted with the EPI-phase correction.

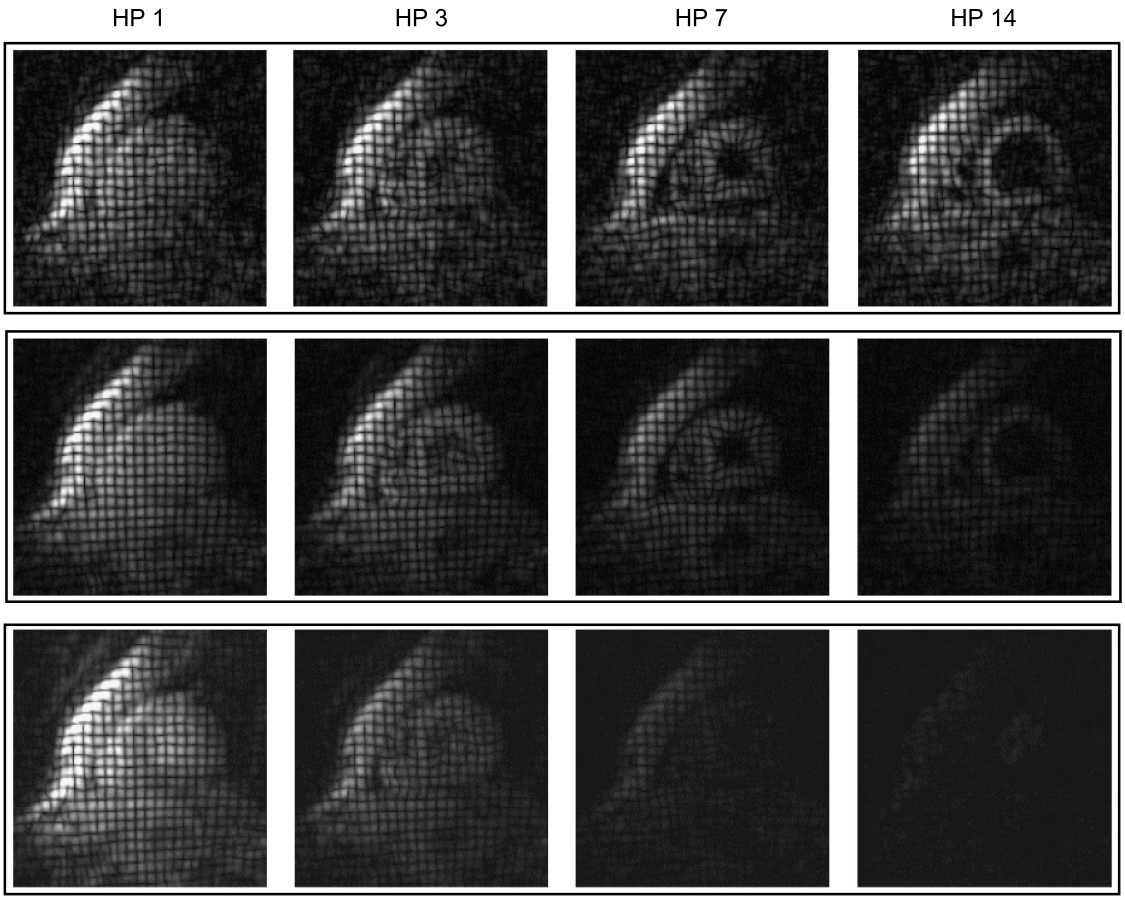

Figure 2. Optimized flip angle scheme. The optimized flip angles lead to a constant tagging contrast over the whole cardiac cycle (upper row) while a constant flip-angle scheme decreases the tagging contrast for later heart phases. Middle row: constant flip angle $\alpha = 8°$, lower row: constant flip angle $\alpha = 25°$. In each row, all four images have the same windowing level.

TAG (x, y) stands for spatial modulation of magnetization,
Δt stands for time between two successive RF-excitations, and
$\alpha_1 \ldots \alpha_n$ stands for RF-excitation angles.

To obtain a constant signal intensity for each acquired cine frame ($I_k = I_{k-1}$), the required flip-angle series $\alpha_1 \ldots \alpha_n$ can be calculated as a function of T_1 and Δt (9):

$$\alpha_{k-1} = \arctan(\sin(\alpha_k) \cdot \exp(-\Delta t/T_1)) \quad \text{for } k = 2 \ldots n \tag{2}$$

In contrast to EPI, where each heart phase is imaged with an individual excitation angle α_i, a variable number of m excitations with excitation angles β_j, $j = 1 \ldots m$ (m: turbo factor) are applied in case of TFEPI. As a result, each β_j excitation must produce an equal amount of transversal magnetization in order to get constant tag-line intensity:

$$\beta_{j+1} = \arcsin(\tan(\beta_j) \cdot \exp(\Delta t/T_1)) \tag{3}$$

The total effect of all β_j flip angles for each heart phase must comply with the α_i excitation for the optimized EPI case (9):

$$\alpha_i = \arccos\left(\prod_{j=1}^{m} \cos(\beta_j)\right) \tag{4}$$

In the example on Fig. 1, ramped flip angles between 3.3° and 13.5° were used to achieve a final flip angle of 25°.

The performance of the flip-angle optimization is shown in Fig. 2. With constant flip angles, the tagging pattern is no longer visible in later heart phases. The application of the optimized flip angles leads to a constant tagging contrast throughout the cardiac cycle.

2.2.2. *Steady-state optimization*

Because of the short acquisition time of the TFEPI sequence, the first image is acquired in a non-steady-state. The subtraction with the complementary image acquired in a

steady-state leads to an alternating tag-line intensity in the final CSPAMM image. To avoid this effect, a dummy RR-interval was introduced in the measurement (i.e., the first image acquired in a transient state of magnetization is subsequently rejected.) In the second RR-interval, the same image is acquired again, but this time in the steady-state and used for subtraction with the complementary image. This procedure prolongs the acquisition of the whole TFEPI-CSPAMM data set by one RR-interval.

Further, in order to not disturb the steady state and to shorten the breath-hold duration, the EPI-reference data for phase correction are acquired in a separate breath hold performed before the actual acquisition. The procedure of this modified TFEPI sequence is illustrated in Fig. 1. In contrast, the EPI and the TFEPI data acquisition is interleaved with the EPI-phase correction.

2.2.3. *Rest measurements*

Seven healthy subjects (5 male, age: 29 ± 5 years) were investigated under rest conditions. CSPAMM images were acquired with an EPI sequence, with a TFEPI sequence with optimized flip angles and with the modified TFEPI sequence including flip-angle and steady-state optimization. The measurements were performed twice in each subject in an equatorial short-axis view.

For both imaging methods, a FOV of 380 × 304 mm^2, a slice thickness of 8 mm, and a final flip angle of 25° were chosen, 20 frames with a temporal resolution of 35 ms were acquired. The EPI-sequence (TE: 7.5 ms, EPI factor: 13, matrix: 128 × 39) had a duration of 12 RR-intervals plus 4 RR-intervals for the EPI phase correction and was acquired in one breath hold. An adaptive flip angle scheme introduced by Stuber et al. (20). was applied. The TFEPI-sequence (TE: 2.6–2.9 ms, TR: 7.1–8.9 ms, EPI factor: 9, turbo-factor: 4, matrix: 128 × 36, partial fourier: 0.67), was combined with the flip-angle optimization described above and had a duration of 4 RR-intervals plus 4 RR-intervals for the EPI correction. With the modified TFEPI-CSPAMM sequence data were acquired in two breath holds lasting 4 and 5 RR-intervals respectively.

2.2.4. *Stress measurements*

Nine healthy subjects (6 male, age: 27 ± 5 years) underwent stress testing. Exercise was performed in the supine position on a MR compatible bicycle ergometer (MRI cardiac ergometer, Lode BV, Groningen, The Netherlands). After the survey, the baseline rest measurements were performed with the modified TFEPI pulse sequence described above.

For the stress measurements, the load was gradually increased until a heartrate of 140 bpm was reached (125–300 W, depending on the training status of the subject), and the volunteer then continued cycling during approximately five minutes at this level of workload.

Imaging was performed again with the modified TFEPI-CSPAMM sequence described above immediately after exercise and at time points 1 minute, 5 minutes, and 10 minutes after exercise. Depending on the heartrate, 10–20 frames (heart phases) with a temporal resolution of 28–36 ms were acquired. In each volunteer, the stress measurements were performed twice applying the same protocol.

2.3. *HARM evaluation*

A magnitude image of the underlying anatomical structure in a tagged image is obtained by filtering k-space to retain a single harmonic peak, applying the inverse Fourier transform

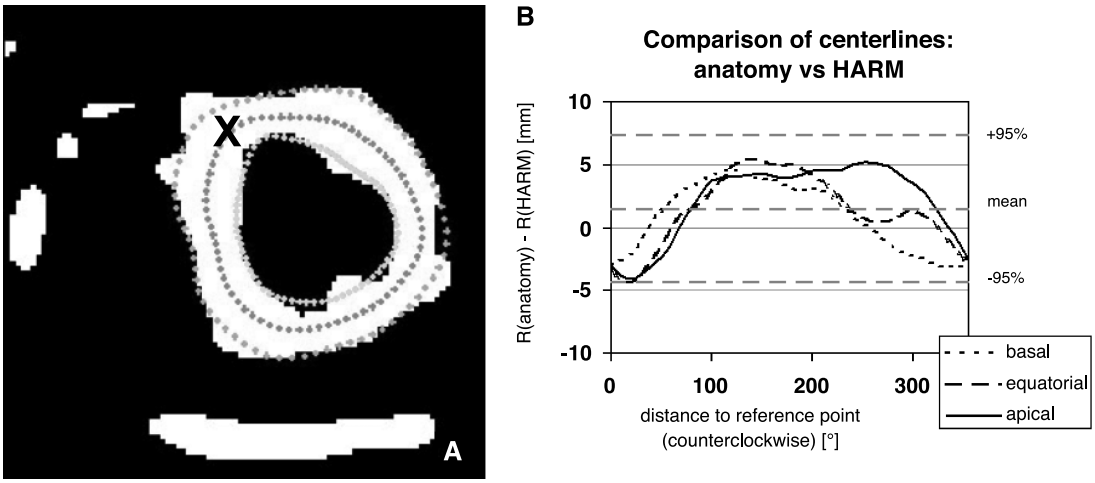

Figure 3. Extraction of anatomical structure in HARM images. The endocardial and epicardial contours are extracted automatically from HARM images and the centerline is calculated. Reference point × (A): Anterior junction of the right and the left ventricle. The centerline determined on HARM images is compared to the centerline extracted from anatomical images (B). The distance to the center (R) of the two centerlines are compared. The difference is displayed along the circumference in steps of 5°. Mean value and the 95% confidence interval are displayed.

and using the magnitude part of the complex image. For a semi-automatic extraction of the endo- and epicardial walls, the observer has to approximate the centerline of the myocardium by setting a few landmarks along its circumference. A closed spline is fitted through these markers and signal intensity along the contour is determined. Starting radially from the center of the contour and in 72 equally distributed directions (approximately 1 per pixel) covering the entire circumference, the application of an adaptive threshold, depending on the mean signal intensity on the spline in a rotating sector surrounding the direction both inside and outside of the contour yields the first guess for the endo- and epicardial contours. Of these initial guesses, outlier landmarks are identified by comparing their distance to the center with the average distance of all landmarks. If the distance difference exceeds two standard deviations the landmark is discarded. The contours are then resampled along a closed spline through the remaining landmarks. Finally, in order to smooth out papillary muscles, the contours are smoothed by averaging the radial distances of the neighbors inside a 45° sector around each landmark. The landmarks are then radially displaced to match the corresponding average distance. Based on these final endo- and epicardial contours, the centerline is finally calculated (Fig. 3A). After the manual definition of the landmarks, the whole computation time is ~2 sec on a pentium 4 1.8 GHz.

In a preliminary study, the centerline extracted semi-automatically from the HARM image was compared with the centerline extracted manually from a corresponding anatomical image. Five hypertensive patients (2 male, age: 63 ± 3 years) with mild left ventricular hypertrophy on echocardiography were recruited for this study. Left ventricular short axis slices were acquired at three cardiac levels. The anatomical images were acquired with an EPI sequence (FOV: 192 × 192 mm^2, slice thickness: 8 mm, matrix: 128 × 80, EPI factor: 9, TE: 4.1 ms). At the same positions, EPI-CSPAMM images were acquired with the protocol described above. For all breath-hold acquisitions, identical position of the heart was achieved by real time navigator control where the subject was guided into the same breath-hold position (acceptance range: ± 1.5 mm of initial diaphragm position). On the anatomical images, the endo- and epicardial contours were delineated manually, on the CSPAMM images the contours were extracted semi-automatically as described above. The centerlines were calculated and the distance between the anatomical centerline and the CSPAMM centerline was determined at 72 positions along the circumference.

Additionally to investigate the reproducibility of deformation parameters extracted by HARP after applying the described method, CSPAMM data acquired in 23 patients with non-ischemic dilated cardiomyopathy at two different time points (2 months apart) were used. [Data from this study analyzed manually were reported by Myers et al. (21)]. The data were acquired on a 1.0 T Philips scanner, spatial resolution: 2.8 × 2.8 mm^2, 16 cardiac phases' temporal resolution: 35 ms, tag distance: 8 mm. To compare inter-observer reproducibility, two observers independently identified the midwall contour manually (22) and semi-automatically as described above. The contour was tracked throughout the cardiac cycle using HARP incorporating peak-combination (23) and maximum cFS was compared. For the calculation of cFS, see below (2.7. HARP evaluation).

2.4. *HARP evaluation*

To extract deformation parameters under rest and stress, HARP evaluation was performed using a peak-combination HARP technique (23) for improved evaluation accuracy. The centerline was semi-automatically defined using the HARM-method as described before, and subsequently tracked over all heart phases.

Circumferential fiber shortening in percent (cFS) was calculated over the cardiac cycle for each sector:

$$cFS(hp) = \left(1 - \frac{CL(hp)}{CL(0)}\right) \cdot 100\% \qquad (5)$$

where hp indicates the heart phase and CL the length of the centerline.

Radial displacement and rotation were calculated with respect to the center of gravity of the centerline. The radial displacement (RD) of each heart phase (hp) is:

$$RD(hp) = \left(1 - \frac{\sum_p |\vec{r}(p,hp)|}{\sum_p |\vec{r}(p,0)|}\right) \cdot 100\% \qquad (6)$$

where $\vec{r}(p)$ is the vector from the dynamic center of gravity (cg) to the point p on the centerline.

The rotation angle ϕ (hp) was defined as the angle between $\vec{r}(p,hp)$ and $\vec{r}(p,0)$ averaged over all p:

$$m(hp) = \frac{y(p,hp) - y(cg,hp)}{x(p,hp) - x(cg,hp)} \qquad (7)$$

$$\phi(hp) = atan\left(\frac{m(hp) - m(0)}{1 + m(0) \cdot m(hp)}\right) \qquad (8)$$

In order to correct for different heart rate, temporal resolution and number of frames, all shortening-, displacement- and rotation-curves were resampled and normalized to end systole (end systole: 100% ES). End systole was defined as the heart phase with the minimal circumference of the centerline.

Circumferential shortening velocity was defined as cFS at end systole divided by the duration of systole.

2.5. *Statistics*

The extracted deformation parameters were compared with an analysis of variance (ANOVA) for repeated measurements followed by Bonferroni posthoc testing (InStat, 3.01,

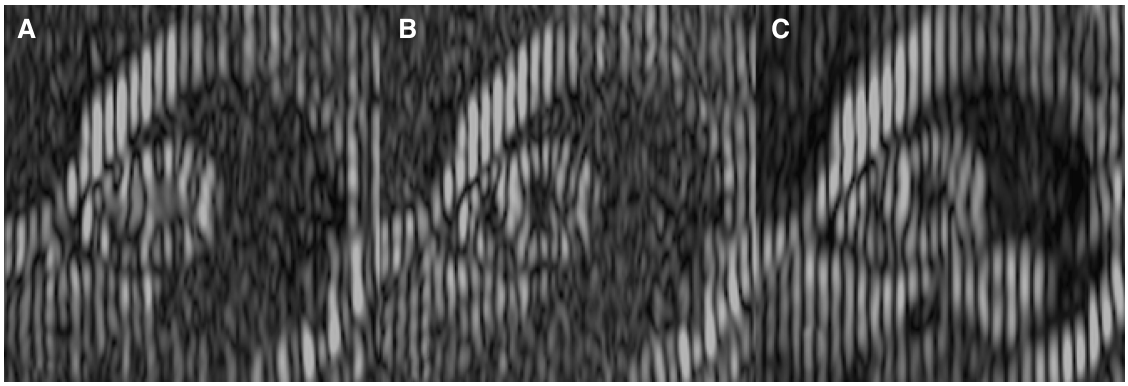

Figure 4. One of two tag-line directions in an equatorial CSPAMM short axis view acquired with a TFEPI sequence (A) a modified TFEPI sequence (B) and an EPI sequence (C). For the TFEPI sequence (A), the alternating tagging pattern can be observed, which is eliminated with the modified TFEPI sequence (B). The image acquired with EPI (C) shows the most homogeneous tagging pattern and less noise.

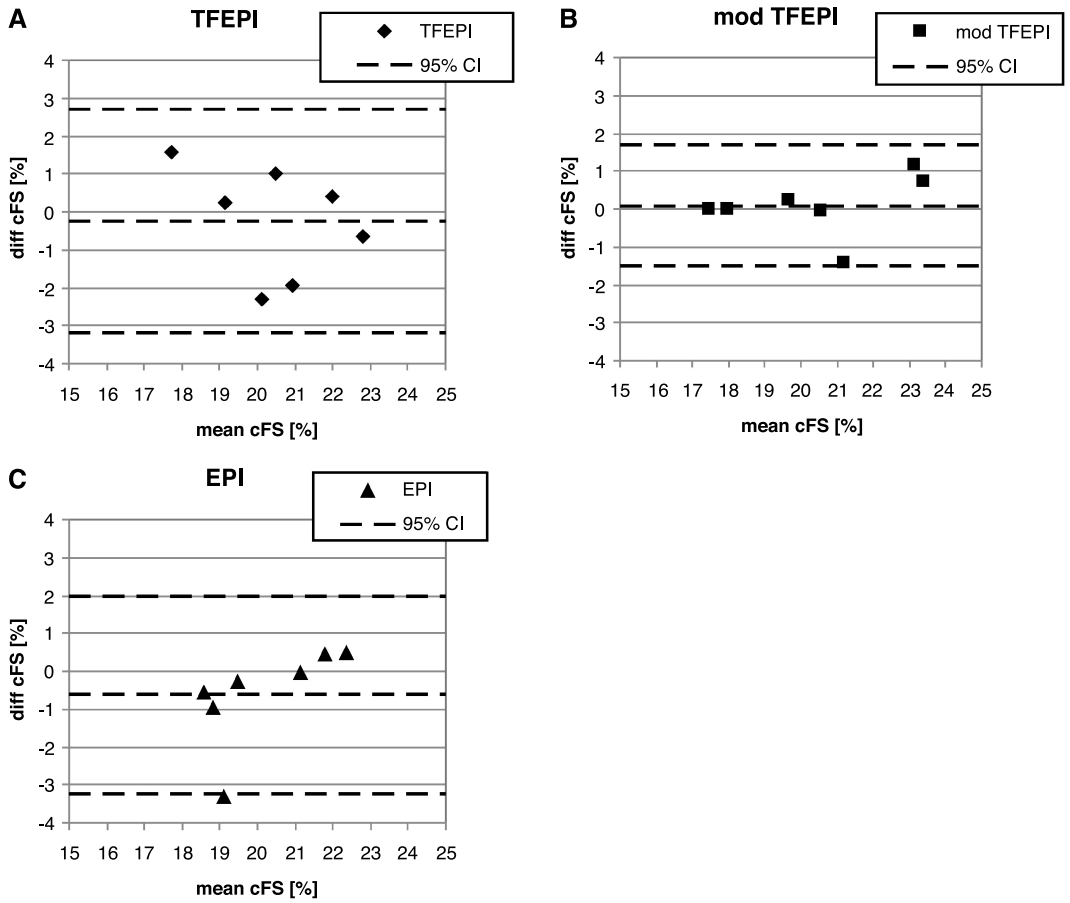

Figure 5. Reproducibility of cFS measurements, A: TFEPI, B: modified TFEPI, C: EPI. The modified TFEPI sequence shows best reproducibility with a 95% confidence interval from −1.5–1.7% of absolute values for the difference between repeated measurements. For the EPI acquisition (C) one subject had difficulties to cooperate adequately during the 16 heart beat breat hold.

Graph-Pad Software Inc.). *P*-values < 0.05 were considered statistically significant.

3. Results

3.1. *TFEPI CSPAMM*

Figure 4 shows examples of short-axis views in a volunteer with the TFEPI- (A), the modified TFEPI- (B) and the EPI- (C) sequence acquired over 8 (1 breath hold), 9 (2 breath holds) and 16 (1 breath hold) heart beats respectively. As expected, an alternating tagging pattern for the TFEPI can be observed (A), whereas the image acquired with the modified TFEPI sequence shows a more homogeneous tagging pattern and a better contrast between blood and myocardium (B). The acquisition with EPI (C) yields the most homogeneous tagging pattern and least noise, provided the subject is able to perform an adequate breath hold over the entire 16 RR acquisition period.

In order to decide which one of the two TFEPI sequences should be used during stress conditions, the sequence performance was compared to the EPI sequence, which served as a state of the art reference (the EPI sequence was not expected to be applicable during stress because of the long breath hold time). A comparison of the maximum cFS of repeated measurements with all three methods is displayed on Fig. 5. While the mean values for repeated measurements are comparable for the three pulse sequences (TFEPI: −0.2%; modified TFEPI: 0.1%; EPI: −0.6%), the 95% confidence intervals, i.e., reproducibility, vary substantially (TFEPI: −3.2–2.7%; modified TFEPI: −1.5–1.7%; EPI: −3.2–2.0% in absolute percentage of cFS). Because of the better performance of the modified TFEPI sequence under rest conditions, it was selected for the measurements under stress conditions.

3.2. *Stress measurements*

In 9 volunteers, a total of 70 stress measurements were performed (4 time points for 2 stress measurements each; due to time constraints, in one volunteer the measurements 10 min after stress were not performed). In one volunteer, cardiac triggering did not work properly during the acquisition performed immediately after ergometer stress. Finally, in two subjects, the stress measurements were performed at an apical position because of a displacement of the subject during cycling. These data were compared with rest data acquired at the apical level.

At time points 0 min, 1 min, 5 min, 10 min after exercise, the heart rate was 118 ± 19 bpm, 98 ± 19 bpm, 79 ± 21 bpm, 74 ± 16 bpm respectively ($p < 0.001$ vs. rest at 0 min, 1 min, $p < 0.01$ at 5 min).

Different deformation parameters were evaluated for all data sets in order to quantify recovery after the stress measurements. In Fig. 6, maximum cFS (A), cFS velocity (B), maximum radial displacement (C) and rotation defined as (*max* (*rot*)−*min* (*rot*)) (D) are displayed during recovery. The maximum cFS at 1 min after exercise differs significantly from maximum cFS at rest ($p < 0.01$), whereas maximum cFS immediately after stress does not differ from rest value.

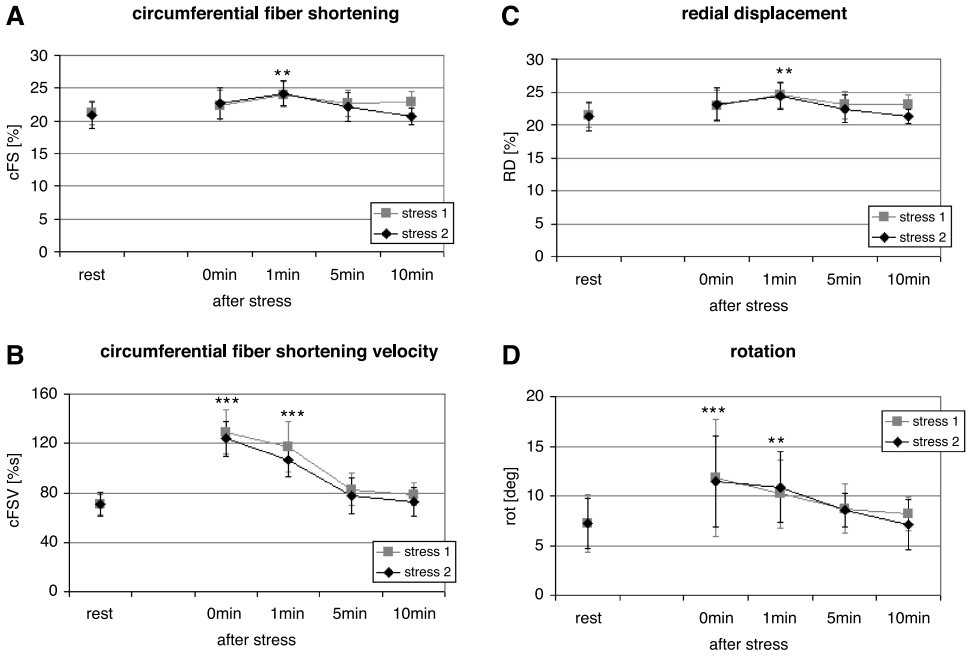

Figure 6. Evolution of peak deformation during recovery acquired with modified TFEPI. The deformation parameters measured after exercise are compared to the rest values. The values that differ significantly from the rest value are indicated (*: $p < 0.05$, **: $p < 0.01$, ***: $p < 0.001$).

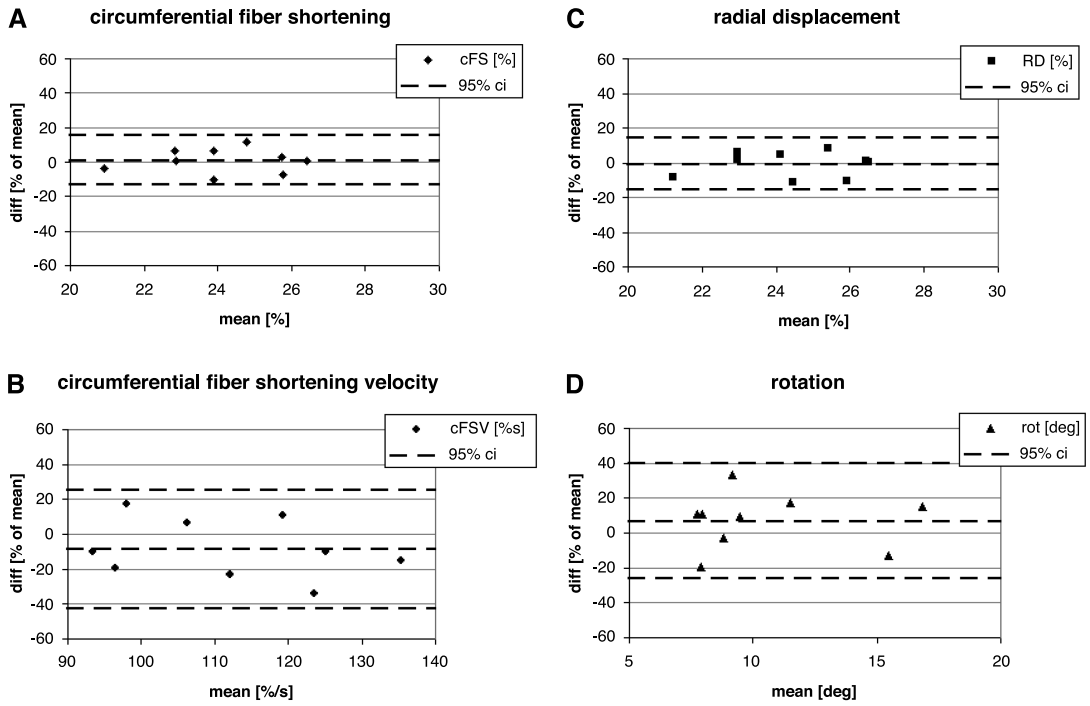

Figure 7. Reproducibility of deformation parameters for repeated measurements. cFS, cFS-velocity, radial displacement and rotation were compared for repeated measurements. The mean value and the 95% confidence interval are indicated on the plot (in units of relative percentage of mean). cFS, acquired with modified TFEPI at a mean heart rate of 100 bpm, shows a high reproducibility with a 95% confidence interval of ± ∼4.0% (absolute percentage of cFS, corresponding to a confidence interval of ± ∼18% for relative percentage of cFS).

Though the cFS velocity is significantly increased compared to rest immediately after exercise ($p < 0.001$) and at 1 min after exercise ($p < 0.001$). Like cFS, the maximum radial displacement differs only 1 min after stress from the rest value ($p < 0.01$), whereas the rotation is elevated immediately after exercise ($p < 0.01$) and 1 min afterwards ($p < 0.05$).

Reproducibility of deformation parameters 1 min after exercise is displayed in Fig. 7. For maximum cFS the 95% confidence interval for repeated measurements is −13.5–15.1% of the mean value, whereas for the rest measurement it is −6.9–7.6% of mean. For cFS velocity the 95% confidence interval is −42.4–25.3% of mean, for radial displacement −15.7–14.1% of mean, and for rotation −25.8–39.5% of mean.

3.3. *HARM evaluation*

Figure 3B shows the difference between the centerlines extracted from the anatomical and the HARM images. The semi-automatically defined centerline is shifted towards the

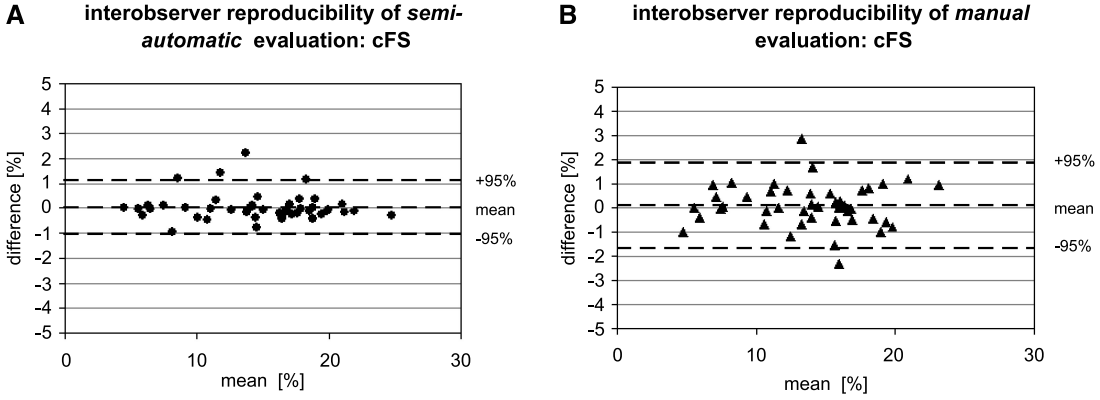

Figure 8. Reproducibility of cFS measurements, automatic vs. manual. The inter-observer reproducibility for the extracted parameters is tested for a manually defined HARM-centerline and a semi-automatically defined HARM-centerline.

endocardium in the free wall and towards the epicardium in the septal wall. The mean difference between the manually and the automatically defined centerlines was 0.9 ± 2.7 mm for the basal, 1.3 ± 2.9 mm for the equatorial, and 2.1 ± 3.0 mm for the apical slices respectively.

The differences of the HARP-analysis between two observers could be reduced by the semi-automatic evaluation and hence inter-observer reproducibility improved. Maximum circumferential shortening differed by 0.08 ± 0.88% for a manually identified contour and by 0.03 ± 0.54% for a contour detected by the algorithm (Fig. 8).

4. Discussion

The goal of our study was to optimize an MR-tagging approach which first allows for a fast data acquisition during a short breath-hold period under stress condition and secondly to provide sufficient quality of these rapidly acquired data for a semi-automatic quantification of various functional indices by HARP.

4.1. *Detection of anatomical structures on tagging data*

Since function parameters vary with varying location within the myocardial wall, e.g., subendo- vs. subepicardial systolic deformation, it is crucial to detect the endo- and epicardial borders in tagging data in order to calculate the centerline. It has been shown previously (24) that deformation parameters extracted from the myocardial centerline give reliable and load-independent measures of myocardial contractility (25, 26). Therefore, we first demonstrated in a preliminary study that the contours defined on HARM images match the contours extracted from anatomical images. This led to a reproducible definition of the centerline improving the overall reproducibility of the HARP evaluation. In this study, only the global cardiac deformation parameters were evaluated. Therefore, the shift of the centerline towards the epicardium in the septal wall (due to the junction with the right ventricle) was compensated by the shift towards the endocardium in the free wall (due to papillary muscles). For an analysis of local motion parameters, these shifts should be considered. The method has only been implemented for short-axis views and would require further development for long-axis views.

4.2. *Optimization of the tagging sequence*

4.2.1. *Rest studies*

The TFEPI sequence was optimized in two steps. First, a flip-angle optimization was applied leading to a constant tagging contrast over the cardiac cycle. In a second step, a dummy RR-interval was introduced for improved image quality. This produced a more uniform tagging pattern and better contrast between blood and myocardium. In a study under rest condition, it was shown that the modified TFEPI sequence performed better with respect to image quality which translated into improved reproducibility of the HARP evaluation. Because of the better performance of the modified TFEPI sequence, it was used for the stress study.

One subject had difficulties performing a breath hold of 16 RR-intervals leading to a worse image quality of the EPI pulse sequence for this subject, and, as a result, reproducibility of the EPI sequence was lower than that of the modified TFEPI sequence. For this reason, the modified TFEPI CSPAMM sequence might be a valid alternative for patients unable to perform long breath holds even under rest condition.

4.2.2. *Stress studies*

The feasibility of using the modified TFEPI-CSPAMM sequence under ergometer stress is demonstrated in the volunteer studies. Except for one acquisition, where ECG triggering failed, all stress data could be evaluated. This suggests that the modified TFEPI-CSPAMM protocol is appropriate for heartrates up to 140 bpm. The cFS velocity was increased immediately after exercise even though maximum cFS was not increased at this time but only 1 min later. The finding that maximum cFS is not augmented for heart rates higher than 100 bpm but for heart rates of approximately 100 bpm is in accordance with earlier findings under dobutamine stress (11). Unlike cFS, rotation did not show a biphasic recovery pattern but decreased steadily following exercise.

While the heart rate was still increased 5 min after exercise, the parameters studied were no longer increased at this time point. This may be explained by the fact that the evaluated deformation parameters describe systolic function and changes in duration of systole with changing heartrate is relatively small compared with duration of diastole.

An ideal parameter describing myocardial mechanics should both, detect subtle changes in mechanics in relation to the stress level and also demonstrate high reproducibility. Such a parameter would allow for reliable detection of altered mechanics in response to changes in stress level. Circumferential shortening reliably discriminates resting conditions from post-stress conditions (at 1 min) and is further characterized by a high reproducibility, i.e., a narrow 95% confidence interval for repeated measurements. Similar observations hold for radial displacement whereas cFS velocity shows a better differentiation between different phases of recovery, however, at the cost of higher variability. For the rotation, although sensitive for altered mechanics, they are less reliable.

4.2.3. *Limitations*

During the stress tests, the goal heart rate for conventional stress examinations, which is normally $0.85 \cdot (220\text{-age [years]})$ bpm, was not achieved. However, it has been shown that for supine bicycle exercise examinations ischemic reactions occur at somewhat lower heart rates ($\sim$110–130 bpm) (27, 28) where the modified TFEPI sequence performed adequately. During exercise a displacement of the subject in

the scanner may occur. This displacement was minimized by a test-cycling prior to starting the MR study.

Since the ECG in the magnet does not allow for assessment of the ST segment, a supervision of the patient might be accomplished by a real-time HARP analysis (29) allowing to detect ischemia during stress. With a contour detection on the HARM images and the fast tagging sequence, the current approach can potentially provide the means for an automatic and reproducible extraction of deformation parameters.

5. Conclusions

A TFEPI-CSPAMM sequence has been introduced, which allows for a fast and reproducible acquisition of cardiac deformation parameters at high heart rates and is, therefore, suitable for measurements under ergometer stress. Despite acquisition times as short as 2 seconds (at 140 bpm), data quality allowed for reproducible semi-automatic quantification of function indices. Further refinements of post-processing are needed to enable objective monitoring and ischemia detection in patients under stress conditions.

Acknowledgments

The authors thank Philips Medical Systems for continuing technical and financial support and ETH Zurich (strategic excellence projects) for financial support.

References

1. de Roos A, van der Wall EE, Bruschke AV, van Voorthuisen AE. Magnetic resonance imaging in the diagnosis and evaluation of myocardial infarction. Magn Reson Q 1991; 7:191–207.
2. van Rugge FP, van der Wall EE, Spanjersberg SJ, de Roos A, Matheijssen NA, Zwinderman AH, van Dijkman PR, Reiber JH, Bruschke AV. Magnetic resonance imaging during dobutamine stress for detection and localization of coronary artery disease. Quantitative wall motion analysis using a modification of the centerline method. Circulation 1994; 90:127–138.
3. Nagel E, Lehmkuhl HB, Bocksch W, Klein C, Vogel U, Frantz E, Ellmer A, Dreysse S, Fleck E. Noninvasive diagnosis of ischemia-induced wall motion abnormalities with the use of high-dose dobutamine stress MRI: comparison with dobutamine stress echocardiography. Circulation 1999; 99:763–770.
4. Pennell DJ, Underwood SR, Manzara CC, Swanton RH, Walker JM, Ell PJ, Longmore DB. Magnetic resonance imaging during dobutamine stress in coronary artery disease. Am J Cardiol 1992; 70:34–40.
5. Turley KR, Wilmore JH. Cardiovascular responses to treadmill and cycle ergometer exercise in children and adults. J Appl Physiol 1997; 83:948–957.
6. Rallidis L, Cokkinos P, Tousoulis D, Nihoyannopoulos P. Comparison of dobutamine and treadmill exercise echocardiography in inducing ischemia in patients with coronary artery disease. J Am Coll Cardiol 1997; 30:1660–1668.
7. Roest AA, Kunz P, Lamb HJ, Helbing WA, van der Wall EE, de Roos A. Biventricular response to supine physical exercise in young adults assessed with ultrafast magnetic resonance imaging. Am J Cardiol 2001; 87:601–605.
8. Axel L, Dougherty L. Heart wall motion: improved method of spatial modulation of magnetization for MR imaging. Radiology 1989; 172:349–350.
9. Fischer SE, McKinnon GC, Maier SE, Boesiger P. Improved myocardial tagging contrast. Magn Reson Med 1993; 30:191–200.
10. Nagel E, Lehmkuhl HB, Klein C, Schneider U, Frantz E, Ellmer A, Bocksch W, Dreysse S, Fleck E. Influence of image quality on the diagnostic accuracy of dobutamine stress magnetic resonance imaging in comparison with dobutamine stress echocardiography for the noninvasive detection of myocardial ischemia. Z Kardiol 1999; 88:622–630.
11. Power TP, Kramer CM, Shaffer AL, Theobald TM, Petruolo S, Reichek N, Rogers WJ Jr. Breath-hold dobutamine magnetic resonance myocardial tagging: normal left ventricular response. Am J Cardiol 1997; 80:1203–1207.
12. Scott CH, Sutton MS, Gusani N, Fayad Z, Kraitchman D, Keane MG, Axel L, Ferrari VA. Effect of dobutamine on regional left ventricular function measured by tagged magnetic resonance imaging in normal subjects. Am J Cardiol 1999; 83:412–417.
13. Geskin G, Kramer CM, Rogers WJ, Theobald TM, Pakstis D, Hu YL, Reichek N. Quantitative assessment of myocardial viability after infarction by dobutamine magnetic resonance tagging. Circulation 1998; 98:217–223.
14. Pedersen EM, Kozerke S, Ringgaard S, Scheidegger MB, Boesiger P. Quantitative abdominal aortic flow measurements at controlled levels of ergometer exercise. Magn Reson Imaging 1999; 17:489–494.
15. Fischer SE, Wickline SA, Lorenz CH. Multiple slice hybrid imaging sequence for myocardial perfusion measurement. In: Proc. Soc. Magn. Reson. New York, USA, 1996:682.
16. Fischer SE, McKinnon GC, Scheidegger MB, Prins W, Meier D, Boesiger P. True myocardial motion tracking. Magn Reson Med 1994; 31:401–413.
17. Osman NF, Kerwin WS, McVeigh ER, Prince JL. Cardiac motion tracking using cine harmonic phase (HARP) magnetic resonance imaging. Magn Reson Med 1999; 42:1048–1060.
18. Kuijer JPA. Myocardial Deformation Measured with Magnetic Resonance Tagging. Vrije Universiteit, 2000.
19. Fischer SE, Wickline SA, Lorenz CH. Novel real-time R-wave detection algorithm based on the vectorcardiogram for accurate gated magnetic resonance acquisitions. Magn Reson Med 1999; 42:361–370.
20. Stuber M, Spiegel MA, Fischer SE, Scheidegger MB, Danias PG, Pedersen EM, Boesiger P. Single breath-hold slice-following CSPAMM myocardial tagging. Magma 1999; 9:85–91.
21. Myers J, Wagner D, Schertler T, Beer M, Luchinger R, Klein M, Rickli H, Muller P, Mayer K, Schwitter J, Dubach P. Effects of exercise training on left ventricular volumes and function in patients with nonischemic cardiomyopathy: application of magnetic resonance myocardial tagging. Am Heart J 2002; 144:719–725.
22. Schwitter J, Ryf S, Spiegel MA, Huerlimann D, Boesiger P. Detection of anatomic structures in MR tagging data: one step further towards automatic tagging analysis. In: ISMRM. Honolulu, 2002:1676.
23. Ryf S, Tsao J, Schwitter J, Stuessi A, Boesiger P. Peak-combination HARP: a method to correct for phase errors in HARP. J Magn Reson Imaging 2004; 20:874–880.
24. Spiegel MA, Luechinger R, Schwitter J, Boesiger P. RingTag: ring-shaped tagging for myocardial centerline assessment. Invest Radiol 2003; 38:669–678.
25. Palmon LC, Reichek N, Yeon SB, Clark NR, Brownson D, Hoffman E, Axel L. Intramural myocardial shortening in hypertensive left

ventricular hypertrophy with normal pump function. Circulation 1994; 89:122–131.
26. Schwitter J, De Marco T, Globits S, Sakuma H, Klinski C, Chatterjee K, Parmley WW, Higgins CB. Influence of felodipine on left ventricular hypertrophy and systolic function in orthotopic heart transplant recipients: possible interaction with cyclosporine medication. J Heart Lung Transplant 1999; 18:1003–1013.
27. Currie PJ, Kelly MJ, Pitt A. Comparison of supine and erect bicycle exercise electrocardiography in coronary heart disease: accentuation of exercise-induced ischemic ST depression by supine posture. Am J Cardiol 1983; 52:1167–1173.
28. Wetherbee JN, Bamrah VS, Ptacin MJ, Kalbfleisch JH. Comparison of st segment depression in upright treadmill and supine bicycle exercise testing. J Am Coll Cardiol 1988; 11:330–337.
29. Sampath S, Derbyshire JA, Atalar E, Osman NF, Prince JL. Real-time imaging of two-dimensional cardiac strain using a harmonic phase magnetic resonance imaging (HARP-MRI) pulse sequence. Magn Reson Med 2003; 50:154–163.